Assessment of concrete fracture parameters using Wedge Splitting Test and Mark Tracking method

Amine JAMAAOUI, Univ. Limoges, GEMH, EA 3178, F-19300 EGLETONS, amine.jamaaoui@etu.unilim.fr

Alexandre GANGNANT, Univ. Bordeaux1, I2M, CNRS UMR 5295, F-33000 BORDEAUX, a.gangnant@i2m.u-bordeaux1.fr

*Ion Octavian POP, Univ. Limoges, GEMH, EA 3178, F-19300 EGLETONS, ion-octavian.pop@unilim.fr

Stéphane MOREL, Univ. Bordeaux1, I2M, CNRS UMR 5295, F-33000 BORDEAUX, s.morel@i2m.u-bordeaux1.fr

Frédéric DUBOIS, Univ. Limoges, GEMH, EA 3178, F-19300 EGLETONS, frederic.dubois@unilim.fr

Abstract:

This paper deals with the characterization of mode I fracture parameters using a kinematic approach integrating the experimental displacement measured by Mark Tracking Method. Tests are carried out using a wedge splitting sample made in concrete. The analysis of the fracture parameters was performed using the Crack Relative Displacement Factor approach and J-integral. By using the optical mark tracking method, the displacement ýeld evolution close to the crack tip is recorded during the test. An adjustment procedure was used to improve the displacement fields and avoid experimental noise. The stress and strain ýelds are calculated using a ýnite element model generated from the experimental displacement ýelds. Further, the energy release rate is evaluated for different crowns deýned around the crack tip and for different loading values.

Keywords: Wedge Splitting Test, opening mode, Mark Tracking method, Energy release rate, Crack Relative Displacement Factor, J-Integral

Nomenclature

A_i^{χ} - weighting coefficients of the power series $\left[mm^{-\chi/2}\right]$

C_1 - reduced elastic compliance $\left[MPa^{-1}\right]$

E - elastic longitudinal modulus $\left[MPa\right]$

f - polar function $\left[rad\right]$

$F_{\max}$ - maximum loading $\left[N\right]$

F_S - vertical load $[N]$

F_V - splitting force $[N]$

G - energy release rate $[N/mm]$

I_i - intensity of grey level of the pixels whose coordinates are (x_1, x_2)

I_s - threshold intensity

J - J-integral $[N/mm]$

$K_1^{(\sigma)}$ - stress intensity factor $\left[MPa \cdot mm^{-1/2}\right]$

$K_1^{(\varepsilon)}$ - crack relative displacement factor $\left[mm^{-1/2}\right]$

l - polar function $[rad]$

N - power series number

r - distance in polar coordinate system $[mm]$

p - index number

R - rigid body rotation $[rad]$

T_1 - rigid body translation in x_1-direction $[mm]$

T_2 - rigid body translation in x_2-direction $[mm]$

u - vector displacement $[mm]$

x_1, x_2 - cartesian coordinate $[mm]$

Greek symbols

α - wedge angle $[rad]$

χ subscript index

ε - strain tensor

φ - angle in polar coordinate system $[rad]$

κ - Kolosovôs constant

ν - Poissonôs ratio

σ - stress tensor $[MPa]$

ξ - residual error $[mm]$

Abbreviations

CCD - Coupled Charge Device

CEA - Commisariat à lôEnergie Atomique

COD ï Crack Opening Displacement

CRDF - Crack Relative Displacement Factor

FE - Finite Elements

LED - Light-Emitting Diode

LVDT - Linear Variable Differential Transformer

ROI ï Region Of Interest

WST ï Wedge Splitting Test

1. Introduction

Cracking is one of the recurring aspects of concrete. Inseparable from its functioning, it can generate pathological consequences. Beyond the aesthetic consequences, it can also reduce the durability of the structure or even affect its behavior, by facilitating the migration of aggressive agents within the material. In these circumstances and considering the relatively high cost of repairs, the structural health assessment of concrete structures must include a strengthening in terms of monitoring of cracks and refine the tools to better identify and quantify the risk of cracking concrete structures.

In recent years, the application of optical techniques in fracture mechanics, for the analysis of kinematic fields and identification of cracking properties continues to grow. They were the object of many developments. In the literature, we distinguish different methods. Among these methods are interferometry and moiré to measure principally the out-of-plane displacement, photoelasticity to evaluate the principal stress, and most recently digital image correlation (DIC) and Mark Tracking techniques to measure the displacement and strain field in-plane [1,2,3,4,5,6]. These optical techniques have been successfully applied in Fracture Mechanics to characterize the cracking process for materials used in civil engineering. Among these methods, the image correlation and mark tracking technique seem most appropriate to characterize the actual displacements and deformations at any point on the surface of the sample. They also provide the ability to generate a finite element mesh from the measurements.

This paper presents an experimental and analytical set up to evaluate fracture parameters loaded in opening mode (mode I) of a sample from the measurements by Mark Tracking method. These field measurements of displacements and deformations are associated with development of an analytical procedure to overcome the experimental errors associated to the presence of the fracture. Thus, we can evaluate the energy release rate via the J-integral.

2. Material and methods

The mechanical behavior was evaluated from Wedge Splitting test [7,8,9,10]. The sample geometry and the set-up of the wedge splitting test is presented schematically in Figure 1. The testing was carried out using an electromechanical press under displacement control. During the test, the applied vertical load component F_V (with $F_S = F_V / \left(2 \cdot \tan\left(\alpha\right)\right)$, and the crack opening displacement (COD) at load line are recorded. The (COD) and loading were measured by means of two LVDT position sensors and a load cell.

In addition with the measurement devices of testing machine, the sample deformation was performed from the measurements by Mark Tracking method [5]. These measurements allowed for determining displacement and strain fields. The Mark Tracking method configuration used consisted of a CCD camera and a LED light source. Deftac software, developed by PEM team of Pprim Institut of Poitiers, was used to perform the mark tracking.

Figure 1. Wedge Splitting Test Setup

WST-specimens were made in concrete. The geometry of WST-cube specimen is shown in Figure 1. The height of the ligament was of 130 mm and length of notch was of 90 mm. Specimens were demoulded after 24h and stored in the water at 19±2 °C until testing. The age at testing was 152 days. Prior testing, the elastic properties of concrete sample were evaluated. The elastic modulus (E) is equal to 37 GPa and Poisson's ratio (ν) is 0.2.

2.1.Mark tracking method

The deformations of sample were measured by the Mark Tracking Method. These measurements allowed for determining displacement and strain fields, and investigate the mode I fracture parameters.

As shown in Figure 2 the basic principle of Mark Tracking Method is based on comparison of two images acquired during the test, one before deformation and another one after deformation [5]. The displacement of each mark is in fact the translation vector (u_1, u_2) in x_1 and x_2 directions of the centre of gravity.

Figure 2. Principle of Mark Tracking Method

Where the centre of gravity coordinates (x_{1g}, x_{2g}) are given by:

$$\begin{Bmatrix} x_{1g} = \dfrac{\sum_i x_i \cdot \left(I_i - I_s\right)}{\sum_i \left(I_i - I_s\right)} \\ x_{2g} = \dfrac{\sum_i y_i \cdot \left(I_i - I_s\right)}{\sum_i \left(I_i - I_s\right)} \end{Bmatrix} \quad (1)$$

Where: I_i is the grey level of the pixels whose coordinates are (x_1, x_2) and I is the threshold value to distinguish the mark.

In our study this optical method was used to measure the kinematic fields on the sample surface. As will be shown later, these marks will be used to calculate fracture parameters.

Figure 3. Mark positions

According to the principle of the mark tracking method illustrated in Figure 3, several black marks are positioned manually on the sample surface. Once the black marks were positioned on the specimen surface, their movement was recorded using the CCD camera during the test. The Region of Interest used to evaluate the fracture parameters was discretized by 437 black marks.

2.2. J ï integral and the Crack Relative Displacement Factor

In order to characterize local or global fracture parameters, several methods have been developed. Among these, the local approach based on Stress Intensity Factor [11,12] and Crack Relative Displacement Factor [13,14] evaluation or the energetic approaches based on energy release rate evaluation via integral invariants [15,16] are the most used ones in fracture mechanics. Based on the possibility to associate the energetic approaches with optical full-ýeld methods in the present study, the fracture phenomenon is characterized using the J-integral

and the CRDF. The advantage of these approaches is the possibility to use the mechanical ýeldsô remote from the crack tip not affected by the crack tip singularity.

Figure 4. Principle of J-integral

Based on the Dubois developments, the kinematic state in the crack tip vicinity can be deýned using CRDF [13,14,17,18]. When considering two opposite points on crack lips identiýed by their polar coordinates (ȝ, ī ´) and (ȝ,+´) (see Fig. 1), the CRDF associated with the opening mode $\left(K_1^{(\varepsilon)}\right)$ can be expressed in terms of relative displacements in x_2 direction:

$$K_1^{(\varepsilon)} = \left|u_2(\xi,-\pi) - u_2(\xi,+\pi)\right| \cdot \sqrt{\frac{2\cdot\pi}{\xi}} \qquad (2)$$

In fracture mechanics, the J-integral is associated with strain energy release rate or the work per unit of crack area. The theoretical concept of the J-integral was developed by [19,20,21,22] who showed that the J-integral is independent of the path deýned around the crack tip (Fig. 4). Thus, the J-integral can be considered as both an energy parameter and a stress intensity parameter. Now, an arbitrary counterclockwise path (Γ) around a crack tip as shown in Figure 4 is considered.

The J-integral can be expressed in the following form:

$$J = \int_{\Gamma} \left\{ \begin{array}{l} \frac{1}{2}\cdot\left[\sigma_{11}\cdot\frac{\partial u_1}{\partial x_1} + \sigma_{22}\cdot\frac{\partial u_2}{\partial x_2} + \sigma_{12}\cdot\left(\frac{\partial u_1}{\partial x_2} + \frac{\partial u_2}{\partial x_1}\right)\right]\cdot n_1 - \\ -\left(\sigma_{11}\cdot\frac{\partial u_1}{\partial x_1} + \sigma_{12}\cdot\frac{\partial u_2}{\partial x_1}\right)\cdot n_1 - \left(\sigma_{12}\cdot\frac{\partial u_1}{\partial x_1} + \sigma_{22}\cdot\frac{\partial u_2}{\partial x_1}\right)\cdot n_1 \end{array} \right\} \cdot ds \qquad (3)$$

Where σ_{ij} and ε_{ij} are the stress and strain tensors. $\vec{n}$ is the unit normal of the contour path, and u is the displacement vector. It should be noted that the crack is oriented in x_1-direction, and the crack tip represents the origin of the coordinate system.

As the analytical forms (2) and (3) show, the CRDF and J-integral evaluation is based on the knowledge of the mechanical ýelds in terms of displacement, strain and stress. Concerning the marks positioned on the specimen surface, they will be used to deýne the Region of Interest and the domain of integration of the J-integral. The mechanical ýelds expressed in equations (2) and (3) will be evaluated from these marks. Therefore, the displacement vector (u) will be evaluated experimentally by mark tracking method, while the strain (ε_{ij}) and stress (σ_{ij}) tensors will be calculated from Finite Element approach. As mentioned above using Mark Tracking method, the ROI can be discretized either by the marks similar to the ýnite element mesh nodes.

3. Results

The general form of force versus displacement graphs is shown in Figure 5.

Figure 5. Force versus displacement

For the present study, we are focused on two loading steps corresponding at 30% of $F_{\max}$ and at $F_{\max}$, respectively.

As mentioned above, in order to calculate fracture parameters, the strain and stress ýeld calculations are performed by ýnite element method using Castem software developed by CEA (Commisariat à lôEnergie Atomiqueð Atomic Energy Commission [23]). For this, the Region Of Interest of WST-specimen has been modeled utilizing the ýnite element method. For this, a ýnite element mesh is generated from Mark Traking measurements. According to the geometrical dimensions of the sample, the mesh is generated using the Cartesian coordinates of the centre of gravity of the marks. Note also that the coordinate system is centred in the crack tip. Taking into account the marks disposition around the crack tip, the ýnite element mesh is generated using four-node quadrilaterals ýnite elements [24,25,26,27] (see Fig. 6). Using all marks, the ýnal mesh contains 437 nodes and 396 four-node quadrilaterals ýnite elements. The displacement field associated to finite element mesh was constructed as a field by point using the experimental displacement.

Figure 6. Finite element mesh

It should be noted that as the black marks are positioned manually on the specimen surface, the regularity and the symmetry of the mesh depend on the precision of the mark position.

Figure 7 represents the experimentally deformed meshes of ZOI corresponding to two loading levels $30\% \cdot F_{\max}$ N and $F_{\max}$ N respectively.

Figure 7. Experimental deformed mesh (Factor scale x300)

Analysis of deformed meshes reveals a light noise of the displacement ýelds and a certain level of displacement symmetry in the x_2-direction, which can be associated with experimental. In order to minimize the effect of experimental measurement uncertainty conditions an adjustment procedure is proposed [13,14,30,31,32]. It should be noted that this adjustment algorithm is based on gap minimization between analytical and experimental displacement ýelds, by use of a iterative Newton Raphson method. Once the experimental displacement calculated, the adjustment procedure is performed between the Williamsô series forms (4) and the displacement fields given by Mark Tracking method. This procedure allowing simultaneous evaluation of the rigid body motion parameters $\left(T_1, T_2, R\right)$ and the series weighting coefficients $\left(A_i^{\chi}\right)$. These parameters are then used to optimize the displacement ýelds by using expression (4).

$$u_1^p = \sum_{\chi=1}^{N}\left(A_1^{\chi}\cdot r_p^{(\chi/2)}\cdot f_{\chi}\left(\kappa,\varphi_p\right)\right) + T_1 - R\cdot x_2^p$$

$$u_2^p = \sum_{\chi=1}^{N}\left(A_1^{\chi}\cdot r_p^{(\chi/2)}\cdot l_{\chi}\left(\kappa,\varphi_p\right)\right) + T_2 + R\cdot x_1^p \qquad (4)$$

$$p = 1..437$$

where N provides the number of terms in the series expansion, A_i are series coefficients, (r,φ) are polar coordinates, $f(k,\theta)$ and $l(k,\theta)$ are the polar functions [13,14,28,29]. The terms T_1, T_2 and R are the rigid body motion. κ is the Kolossov constant defined according with plane stress configuration [13,14,28,29]. The index ñpò corresponds to analyzed mark number.

It should be noted that the choice of degree of interpolation (i.e. number of terms in the series expansion) is driven by the minimization of residual error ξ :

$$\xi = \frac{\sum_{p=1}^{437}\left(\left|u_1^p - u_1^{\exp erimetal}\right| + \left|u_2^p - u_2^{\exp erimetal}\right|\right)}{437} \tag{5}$$

In the present study, we set $N = 7$ as the value at which error is minimized $\left(\xi_{30\%\cdot F_{\max}} = 0.12\,mm; \xi_{F_{\max}} = 0.07\,mm\right)$.

The deformed meshes performed by means the adjustment procedure have been illustrated in Figure 7.

Figure 8. Deformed mesh using adjusted displacement (Factor scale x300)

Now, using the adjusted displacement fields the fracture parameters in terms of CRDF and J-integral was performed.

As mentioned above in opening mode the Crack Relative Displacement Factor may be performed using the displacement fields near to the crack tip (equation (2)).The method employed is based on an image of the crack lip kinetics, as given by the relative displacement factor of two opposite points placed on the crack lips at a distance (ξ) from the crack tip.

The recent works [13,14] have shown also that this factor may be calculated from the first weighting coefficient A_1^1 of the Muskhelishvili series (4).

$$K_1^{(\varepsilon)} = A_1^1 \cdot (\kappa + 1) \cdot \sqrt{8 \cdot \pi} \tag{6}$$

Moreover, by applying the superposition principle, Dubois shows that by separating the relative displacement description from the stress distribution the energy release rate may be expressed in the fallowing form [13,14,17,18]:

$$G_1 = \frac{1}{C_1} \cdot \left(K_1^{(\varepsilon)} \right)^2 ;$$
$$where:$$
$$K_1^{(\varepsilon)} = C_1 \cdot K_1^{(\sigma)} \qquad (7)$$
$$C_1 = 8 / E$$

Where $K_1^{(\sigma)}$ is the stress intensity factor.

Then, the fracture parameter obtained from a local approach using the kinematic fields are given in Table 1:

Tableau 1. Fracture parameters from kinematic field

By using the ýnite elements approach and the experimental data, the J-integral is evaluated numerically via equation (4). According with the principle of J-integral the domain of integration is assimilated by crowns deýned by the black marks positioned around the crack tip (see Fig. 9). As indicated above the strain and stress ýeld calculations are also performed by ýnite element method. It should be noted that according to J-integral calculation, the specimen geometry is rotated in order to align the crack with x_1-direction.

Figure 9. Crowns of integration surrounding the crack tip

The J-integral values versus size of the domain of integration are presented in Table 2.

Tableau 2. J ï integral versus Γ

Comparison between the energy values obtained by CRDF (Table 1) approach and J-integral (Table 2) reveals a good agreement. This analysis lead us to conclude that the Crack Relative Displacement factor approach provides a good estimation of energy release rate compatible with the J-integral approach. This approach allows to consider the assessment of fracture parameters for the real structures.

4. Conclusion

In this study, we have proposed a coupling between experimental and numerical approaches for the purpose of characterizing fracture parameters in an opening mode conýguration. Based on the experimental optical measurements, the energy release rate was performed by means two methods, Crack Relative Displacement Factor and J-integral, respectively. The Mark Tracking method is employed in order to measure the displacements ýelds. Using the experimental displacement and the strain ýelds, the stress tensor is calculated by finite element approach via a constitutive law. For this purpose, the experimental data are implemented in a ýnite element code in order to generate a ýnite element mesh. Using the mechanical ýelds measured or evaluated by coupling experimental with numerical approaches, the CRDF and J-integral were calculated.

This study lead us to conclude that the mark tracking method may be adapted to implement the experimental measurements in a ýnite element code in order to generate the ýnite element mesh. This possibility can be explored to generate meshes of the complex geometry of specimens. Implementation of the experimental data in the ýnite elements codes allows also to obtain a realistic discretization of the experimental specimens. The present study allows also to conclude that the Crack Relative Displacement factor approach provides a good estimation of energy release rate. This approach allows to consider the assessment of fracture parameters for the real structures.

References

[1] D. Post, Moire interferometry. In: Kobayashi AS (ed) Handbook on experimental mechanics, VCH Publishers Inc, New York, 1993.

[2] A. Wells, D. Post, The dynamic stress distribution surrounding a running crackð a photoelastic analysis, *Proc Soc Exp Stress Anal* 16 (1958) 69ï 92.

[3] M.A. Sutton, W.J. Wolters, W.H. Peters, W.F. Ranson, S.R. McNeil, Determination of displacements using an improved digital correlation method, *Image Vision Comput* 1 (1983) 133ï 139.

[4] F. Hild, S. Roux, Measuring stress intensity factors with a camera: integrated digital image correlation (I-DIC), *Comptes Rendus Mécanique* 334 (2006) 8ï 12.

[5] N. Bretagne, V. Valle, J.C. Dupre, Development of the marks tracking technique for strain ýeld and volume variation measurements, *NDT&E Int* 38 (2005) 290ï 298.

[6] J.J. Orteu, 3-D computer vision in experimental mechanics, *Opt Laser Eng* 47 (2009) 282ï 291.

[7] I. Löfgren, H. Stang, J.F. Olesen, The WST method, a fracture mechanics test method for FRC, *Mater Struct* 41 (2007) 197ï 211.

[8] H. Harmuth, K. Rieder, M. Krobath, E. Tschegg, Investigation of the nonlinear fracture behaviour of ordinary ceramic refractory materials, *Mater Sci Eng A* 214 (1996) 53ï 61.

[9] X.Z. Wang, Z.C. Xu, Z. Bi, H. Wang, Experimental investigation on relative crack length for fracture toughness of concrete, *Adv Mater Res* (2010) 146ï 147.

[10] E. Brühwiler, F.H. Wittmann, The wedge splitting test, a new method of performing stable fracture mechanics tests, *Eng Fract Mech* 35 (1990) 117ï 25.

[11] D. Broek, Elementary engineering fracture mechanics, Kluwer, Dordrecht, 1974.

[12] R.J. Sanford, Fracture mechanics, ASTM STP 833, 1982.

[13] M. Méité, F. Dubois, O. Pop, J. Absi, Mixed mode fracture properties characterization for wood by Digital Images Correlation and Finite Element Method coupling, *Engineering Fracture Mechanics* 105 (2013) 86-100.

[14] M. Méité, O. Pop, F. Dubois, J. Absi, Characterization of mixed-mode fracture based on a complementary analysis by means of full-field optical and finite element approaches, *International Journal of Fracture*, 180 (2013) 41-52.

[15] B.D. Vujanovic, T.M. Atanackovic, An introduction to modern variational techniques in mechanics, Birkhaüser, Switzerland, 1930.

[16] C. Lanczos, The variational principles of mechanics, 4th edn. Dover Publications, New York, 1970.

[17] F. Dubois, C. Chazal, C. Petit, Viscoelastic crack growth Process in wood timbers: an approach by the ýnite element method For mode I fracture, *Int J Fract* 88 (2002) 113-367.

[18] F. Dubois, C. Petit, Modelling of the crack growth initiation in viscoelastic media by the Gtheta integral, *Engng Fract Mech* 36 (2005) 72 - 2821.

[19] G.P. Cherepanov, The stress in a heterogeneous plate with slits, in Russian, *Izvestia AN SSSR, OTN, Mekhan. I Mashin* 1 (1962) 131ï 137.

[20] G.P. Cherepanov, Mechanics of brittle fracture, McGraw-Hill, New York, 1979.

[21] J.R. Rice, A path independent integral and the approximate analysis of strain concentration by notches and cracks, *J Appl Mech* 35 (1968) 379ï 386.

[22] B. Budiansky, J.R. Rice, Conservation laws and energy-release rates, ASME *J Appl Mech* 40 (1973) 201ï 203.

[23] E. Le Fichoux, Presentation and use of Castem 2000 (In French), ENSTA-LME, 1998.

[24] J. Bathe, J. Klaus, Finite element procedures in engineering analysis, Prentice-Hall, Englewood, 1982.

[25] O.C. Zienkiewicz, R.L. Taylor, The ýnite element method for solid and structural mechanics, Elsevier Butterworth Heinemann, Amsterdam, 2005.

[26] T.S. Anderson, Fracture mechanics. CRC Press, Boca Raton, FL, 2005

[27] O. Pop, F. Dubois, J. Absi, J-integral evaluation in cracked wood specimen using the mark tracking method, *Wood Sci Technol* 47 (2013) 257ï 267.

[28] N.I. Muskhelishvili, Some basic problem of mathematical theory of elasticity, English translation, Noordhoff 1933.

[29] M. Williams, On the stress distribution at the base of a stationary crack, ASME Journal Applied Mechanics 24 (1957) 109-114.

[30] H.A. Bruck, S.R. McNeill, M.A. Sutton, W.H. Peters, Digital image correlation using Newtonï Raphson method of partial differential correction, *Exp. Mech.* 29 (1989) 261ï 267.

[31] S. Yoneyama, Y. Morimoto, M. Takashi, Automatic Evaluation of mixed-mode stress intensity factors utilizing digital image correlation, *Strain* 42 (2006) 21-29.

[32] S. Yoneyama, T. Ogawa, Y. Kobayashi, Evaluating mixed-mode stress intensity factors from full-field displacement obtained by optical methods, *Engineering fracture mechanics* 74 (2007) 1399-1412.

Figures

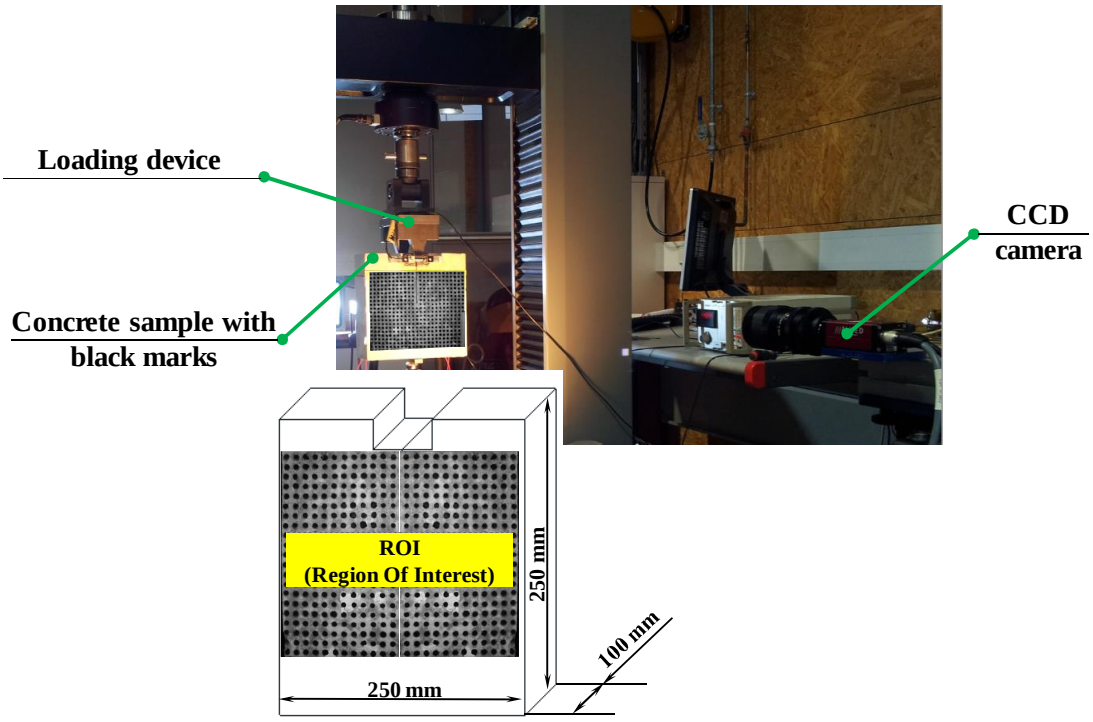

Figure 1. Wedge Splitting Test Setup

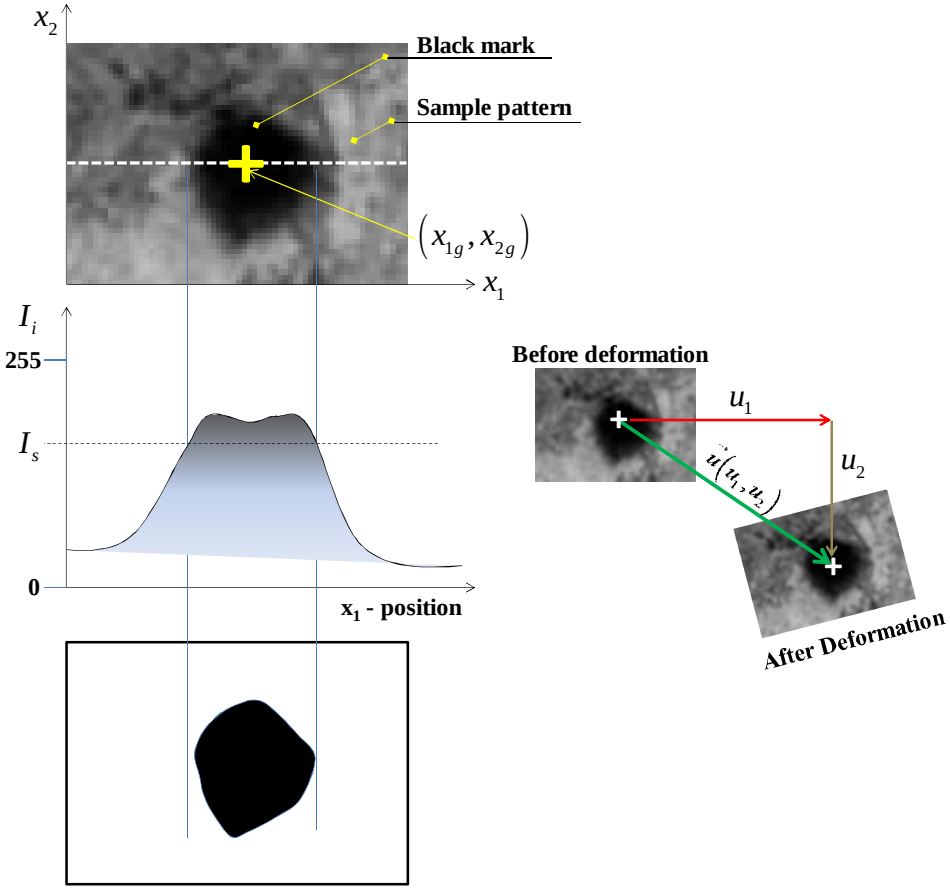

Figure 2. Principle of Mark Tracking Method

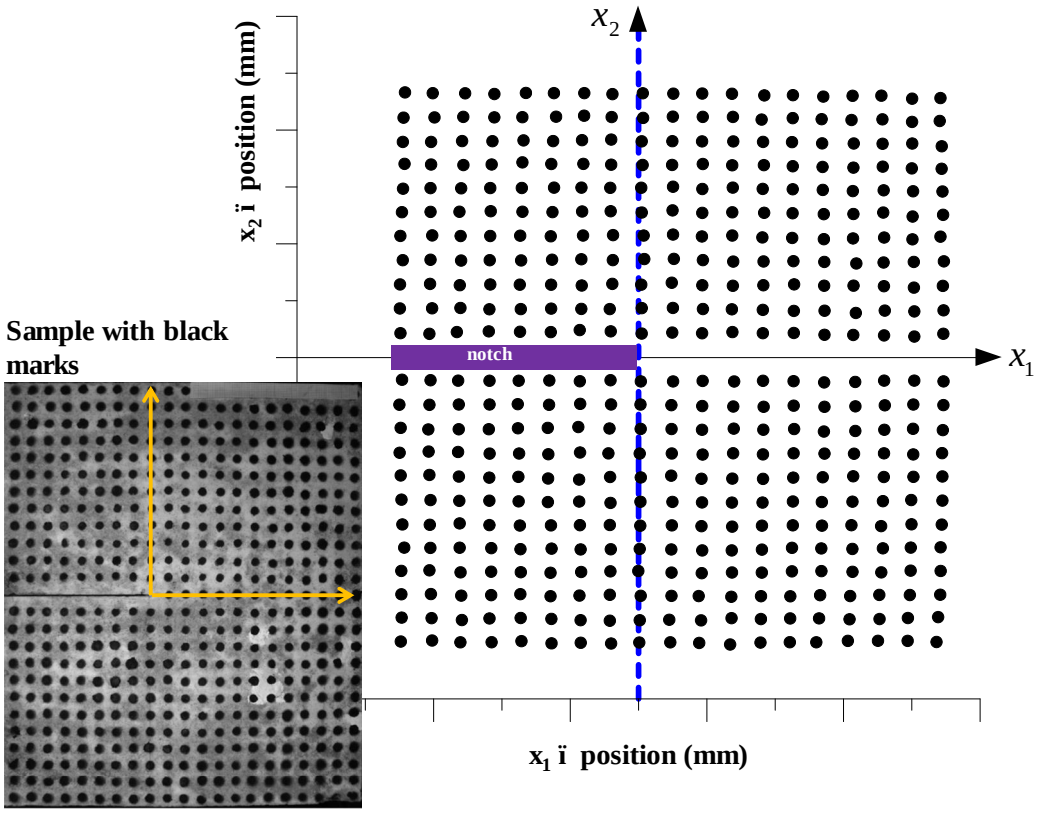

Figure 3. Mark positions

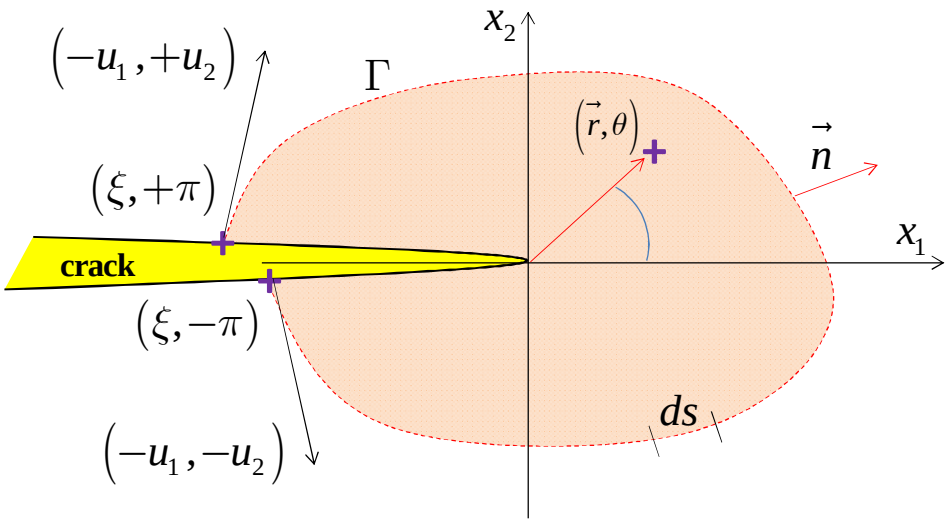

Figure 4. Principle of J-integral

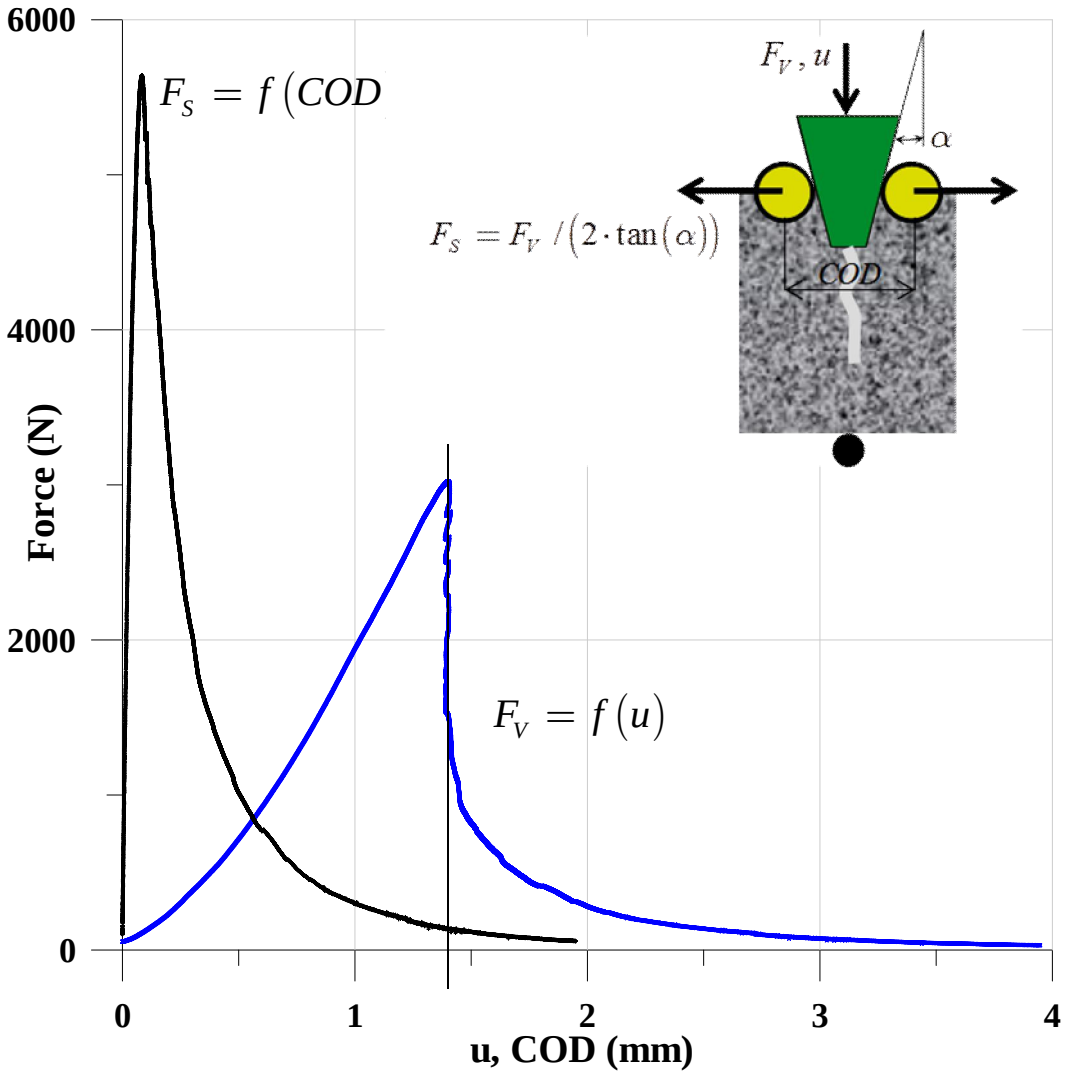

Figure 5. Force versus displacement

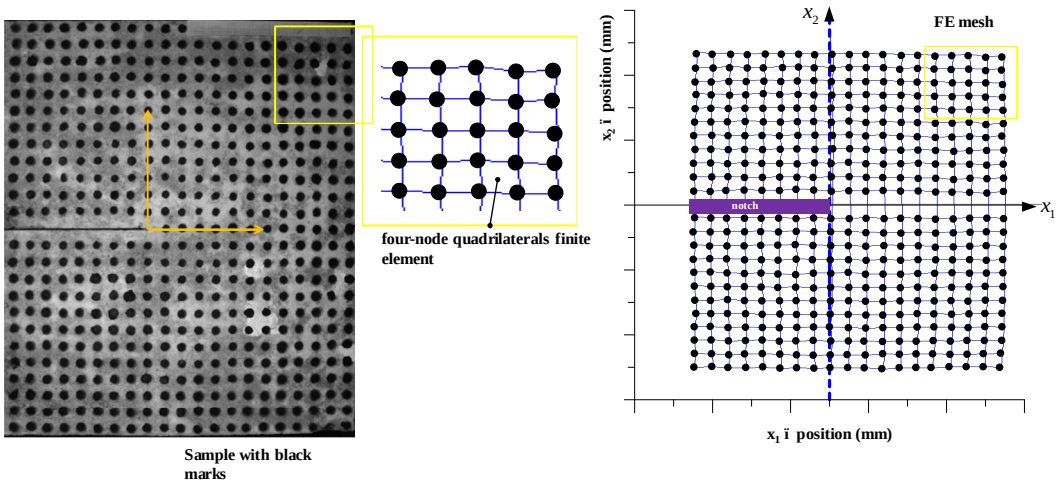

Figure 6. Finite element mesh

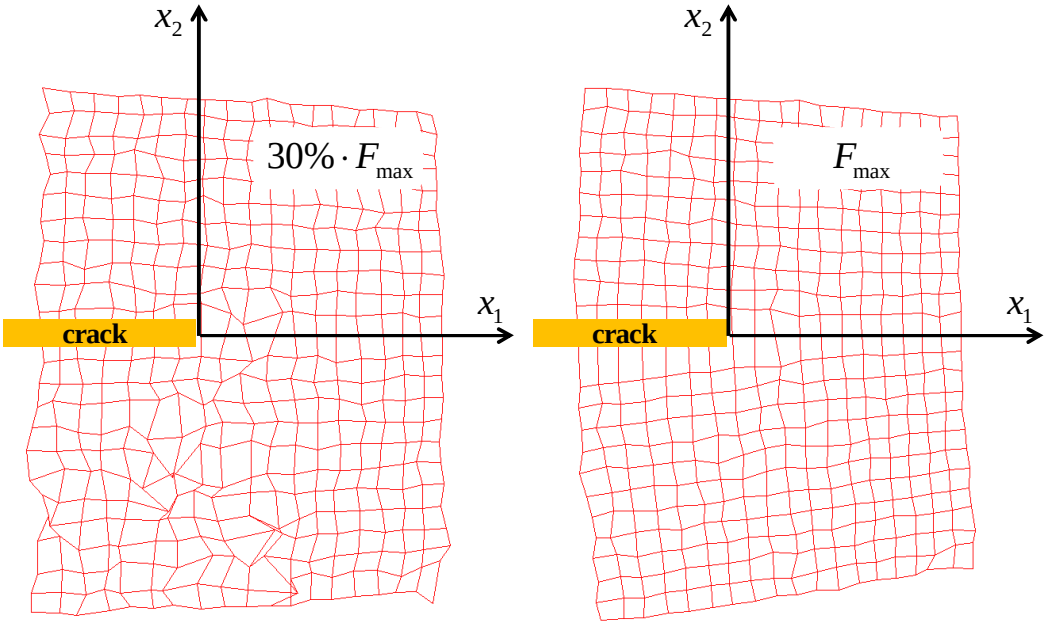

Figure 7. Experimental deformed mesh (Factor scale x300)

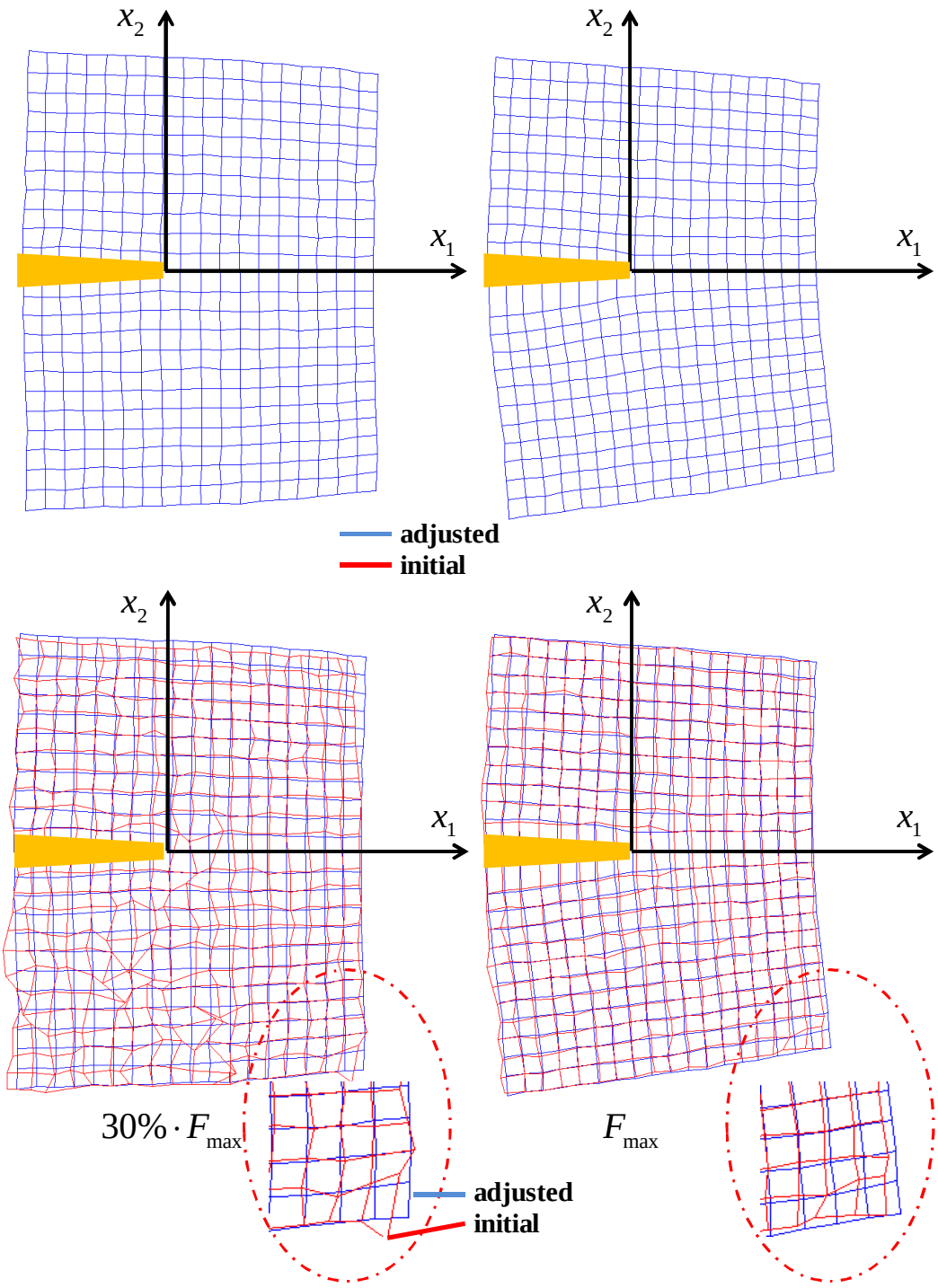

Figure 8. Deformed mesh using adjusted displacement (Factor scale x300)

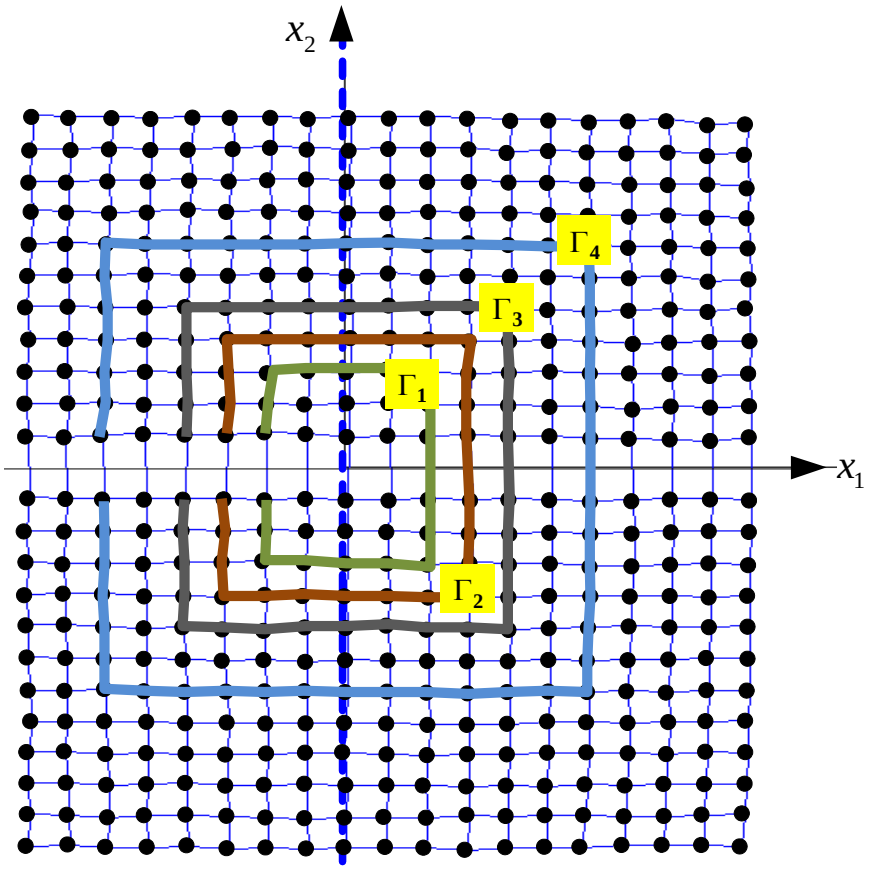

Figure 9. Crowns of integration surrounding the crack tip

Tables

Tableau 1. Fracture parameters from kinematic field

Loading	$K_1^{(\varepsilon)}\ \left(\sqrt{mm}\right)$	$K_1^{(\sigma)}\ \left(MPa\cdot\sqrt{mm}\right)$	$G\ \left(N/mm\right)$
$30\%\cdot F_{\max}$	0.0025	11.58	0.0290
$F_{\max}$	0.0033	15.44	0.0515

Tableau 2. J ï integral versus Γ

Loading	J ï integral (N/mm)			
	Γ_1	Γ_2	Γ_3	Γ_4
$30\% \cdot F_{\max}$	0.0287	0.0286	0.0287	0.286
$F_{\max}$	0.0518	0.0516	0.0518	0.0516